Mixed-Layer Depth Model Based on Turbulent Energetics[1]

ROLAND B. STULL[2]

Department of Atmospheric Sciences, University of Washington, Seattle 98195

(Manuscript received 10 October 1975, in revised form 29 March 1976)

ABSTRACT

Mixed layer depths are predicted using an entrainment equation with conservation equations. The entrainment equation is based on the turbulent kinetic energy equation for the mixed layer. The atmosphere is idealized as having temperatures, humidities and winds constant with height in the boundary layer with a step discontinuity marking the top of the mixed layer. This model is tested with mixed layer depth observations made during the 1953 Great Plains experiment, the 1967 Australian Wangara experiment, and the 1972 Puerto Rican tropical experiment. Model calculations of inversion rise and mixed layer depth offer good agreement with the observations. It is found that none of the turbulence generation and loss mechanisms for the mixed layer (such as buoyancy, wind shear and gravity waves) should be neglected *a priori*.

1. Introduction

Atmospheric mixed layers often change in thickness during the course of a day. The base of the temperature inversion capping the mixed layer thus rises and descends. The goal of this paper is to build a predictive model describing the variations of the mixed layer depth with time.

An important property of a temperature inversion is its static stability. In this paper, a temperature inversion is defined as a layer of air with virtual potential temperature increasing with height. Fig. 1 of Stull (1976a) shows the idealized characteristics of a well-mixed atmospheric boundary layer capped by a temperature inversion. Note that a temperature jump exists at the base of this idealized inversion, while the virtual potential temperature of the mixed layer is constant with height.

This idealized picture agrees fairly well with laboratory and field observations: Lettau and Davidson (1957), Neiburger *et al.* (1961), Izumi (1964), Deardorff and Willis (1967), Turner (1968), Deardorff *et al.* (1969), Mendonca and Iwaoka (1969), Lenschow (1970, 1973, 1974), Clarke *et al.* (1971), Cattle and Weston (1973), Pennell and LeMone (1974), Willis and Deardorff (1974), McEwan and Paltridge (1976), and many others.

Many investigators have proposed theoretical models for geophysical mixed layers bounded by stable layers; some for oceanic mixed layer/thermocline systems (Rouse and Dodu, 1955; Kraus and Turner, 1967; Miropol'skiy, 1970; Pollard *et al.*, 1973), and others for atmospheric boundary layer/inversion systems (Ball, 1960; Fleagle and Businger, 1963; Lilly, 1968; Geisler and Kraus, 1969; Zilitinkevich, 1972, 1975a, b; Betts, 1973a, b; Carson, 1973; Deardorff, 1973, 1974a, b; Stull, 1973, 1975; Tennekes, 1973, 1975; Orlanski *et al.*, 1974; Wyngaard and Coté, 1974; Zilitinkevich and Deardorff, 1974; Drake *et al.*, 1975; Manton, 1975; Mahrt and Lenschow, 1976).

Most investigators use similar basic equations: conservation of mass, heat, moisture, momentum, and the equation of state. They differ in their assumption concerning entrainment of stable fluid into the mixed layer—an assumption which must be made to close their equations.

Investigators often model special cases such as free convection, forced convection, or Kelvin-Helmholtz waves in order to simplify their entrainment equation. For example, one free convection entrainment assumption is

$$(\overline{w'\theta'})_h = -A_1(\overline{w'\theta'})_s,$$

where $\rho C_p(\overline{w'\theta'})$ is a turbulent heat flux, A_1 an empirical constant, ρ the mean air density, C_p the specific heat of air, w vertical velocity, θ potential temperature, and the subscripts h and s apply to the inversion base and the earth's surface, respectively.

Examples of observed and postulated values of A_1 are compiled by Stull (1976a). One notes that values for A_1 range between zero and 1, although most lie between 0.1 and 0.3. It is shown later in this paper that many processes such as buoyant convection and

[1] Contribution No. 374, Department of Atmospheric Sciences, University of Washington.

[2] Present affiliation: Air Force Global Weather Central, Offutt AFB, Omaha, Neb. 68113.

wind shear operate simultaneously in the atmosphere; hence, the large variation in A_1 reflects the unjustified neglect of some of these processes.

In this paper, all relevant processes will be considered and included in the entrainment assumption. This entrainment equation is derived in companion papers (Stull, 1976a, b); it is referred to here as the energetics theory. Basic equations are briefly summarized in the next section. Then, these equations together with the energetics entrainment equation are tested in several case studies against observed atmospheric mixed layer data.

2. Basic equations summary

Following Stull (1975), we write the conservation of mass for the mixed layer (assumed incompressible) as

$$\frac{dh}{dt}=w_e+(w_s+w_{sc}),$$

where h is the inversion base height (depth of the mixed layer), w_e the entrainment velocity (rate of volume entrained per unit area), w_s the synoptic-scale vertical velocity at h (negative for subsidence), and w_{sc} reflects any cloud-induced subsidence. The synoptic-scale velocity w_s, a specified boundary condition, is approximated by $w_s=-Bh$, where B is the large-scale divergence (Stull, 1973). For simplicity, B is assumed to be a different constant in each different case study.

The first law of thermodynamics integrated over the mixed layer depth is

$$h\frac{d\hat{\theta}}{dt}=(\overline{w'\theta'})_s-(\overline{w'\theta'})_h+\frac{h\theta}{C_pT}\hat{Q},$$

where T is the absolute temperature, Q the heating rate due to infrared radiation, and the caret indicates an average over the depth of the mixed layer.

Similarly, the integrated conservation equation for moisture is

$$h\frac{d\hat{\rho}_w}{dt}=(\overline{w'\rho_w'})_s-(\overline{w'\rho_w'})_h,$$

where ρ_w is the absolute humidity and $\overline{w'\rho_w'}$ are the turbulent moisture fluxes.

The virtual potential temperature θ_v and virtual heat fluxes $(\overline{w'\theta_v'})$ are approximated as

$$\left.\begin{aligned}\theta_v&\approx\theta(1+0.61q)\\(\overline{w'\theta_v'})&\approx\overline{w'\theta'}(1+0.61q)+0.61\theta\overline{w'q'}\end{aligned}\right\},$$

where q is the specific humidity $[q\approx\rho_w/(\rho_w+\rho_{AIR})]$. The free convection scaling w_* is

$$w_*^3\equiv(gh/\theta_{v0})(\overline{w'\theta_v'})_s$$

and γ is the virtual potential temperature lapse rate just above h.

Integrating the momentum conservation equation over h yields

$$h\frac{d\hat{u}}{dt}=-hf(\hat{v}_g-\hat{v})+(\overline{u'w'})_s-(\overline{u'w'})_h,$$

$$h\frac{d\hat{v}}{dt}=hf(\hat{u}_g-\hat{u})+(\overline{v'w'})_s-(\overline{v'w'})_h,$$

where

$$(\overline{u'w'})_s=-C_D\hat{u}|\hat{u}|$$

$$(\overline{v'w'})_s=-C_D\hat{v}|\hat{v}|$$

$$C_D=5\times10^{-4}[1+0.07M]\left[1+20\left(\frac{w_*}{M}\right)^{\frac{3}{4}}\right]$$

$$M^2=\hat{u}^2+\hat{v}^2$$

$$(\Delta u_h)^2=(\Delta u)^2+(\Delta v)^2.$$

The drag coefficient follows from the expression designed by Deardorff (1968).

All of the turbulent fluxes at h are written as

$$-(\overline{w'\phi'})_h=w_e\Delta\phi,$$

where $\Delta\phi$ is the jump of the arbitrary variable ϕ at the inversion base. Most of the surface fluxes are boundary conditions which must be specified.

The infrared heating is found from the net radiational flux (F_n) divergence

$$Q=-\frac{1}{\rho_0}\frac{\partial F_n}{\partial z}.$$

A flux emissivity (ϵ) approach (water vapor only) using the radiation tables of Staley and Jurica (1970) approximates F_n at any level by

$$F_n=\int_0^{\epsilon_B}\sigma T^4d\epsilon-\int_0^{\epsilon_T}\sigma T^4d\epsilon+(1-\epsilon_B)\sigma T_{\text{surf}}^4,$$

where σ is the Stefan-Boltzman constant, and the subscripts B and T denote the bottom and top of the troposphere, respectively.

The energetics entrainment rate equation (Stull, 1976a) is

$$w_e=\underbrace{A_1\frac{(\overline{w'\theta_v'})_0}{\Delta\theta_v}}_{\text{I}}+\underbrace{A_2\frac{\theta_{v0}u_*^2|\hat{u}|}{gd_1\Delta\theta_v}}_{\text{II}}+\underbrace{A_3\frac{\Delta u_h}{\text{Ri}_B}}_{\text{III}}-\underbrace{\text{GW}\left(\frac{2\theta_{v0}}{gd_1\Delta\theta_v}\right)}_{\text{IV}},\quad(1)$$

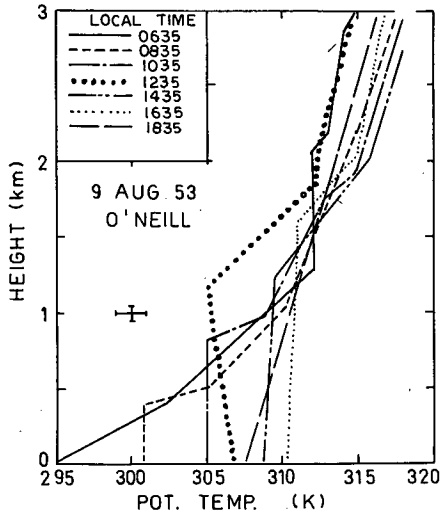

FIG. 1. Observed inversion rise as shown by potential temperature soundings.

where

$$A_1=0.10\pm0.05,$$
$$A_2=0.05\pm0.025,$$
$$A_3=0.001\pm0.0005.$$

Note that the values of these coefficients were found by trial and error to give the best results of predicted inversion rise for two cases: 25 August 1953 at O'Neill and Day 33 of the Wangara experiment. These same "best values" were then used in four other case studies with excellent results (Stull, 1975): 9 and 19 August 1953 at O'Neill, 15 December 1972 at Puerto Rico, and a laboratory tank analogy case. Out of those six cases, only three are discussed in this paper. (See Fig. 7 for descriptions of the terms I–IV and their contribution to the total entrainment velocity.)

The bulk Richardson number is

$$\mathrm{Ri}_B=\frac{g(\Delta\theta_v/\theta_{v0})d_1}{\Delta u_h^2},$$

and d_1 is found by

$$\frac{d_1}{h}=\frac{w_e\Delta\theta_v}{\overline{(w'\theta_v')}_s+w_e\Delta\theta_v}.$$

The energy flux lost due to gravity waves (GW) is discussed by Stull (1976b).

Convective clouds are assumed to form when the top of the mixed layer reaches saturation. Following Betts (1973b) and Sarachik (1974), it is assumed that the fraction of area covered by clouds reaches an equilibrium point where the sum of cloud-induced subsidence, synoptic-scale subsidence and entrainment is zero. The mixed layer depth then ceases to change except for changes in cloud base height caused by changes in the mean humidity of the mixed layer.

It is assumed for simplicity that the upward vertical velocity w_{CLD} into the cloud base is nearly a constant for fair weather cumulus clouds. With this assumption, the steady-state continuity equation applied at cloud base gives

$$\sigma=\frac{w_e-w_s}{w_e+w_{\mathrm{CLD}}},$$

where σ is the fraction of area covered by active convective clouds.

The fields of temperature and humidity above h are modified by advection, subsidence ($w_s=-Bz$) and

TABLE 1. Values of the parameters used in the case studies.

Parameter description	Symbol	Sensitivity test	Case studies O'Neill	Wangara	Puerto Rico
1. Time increment	TI (s)	300.	120.	120.	120.
2. Number of time steps between radiation calculations	SKIPP (2)	60.	60.	60.	60.
3. Average mixed layer geostrophic wind components (m s^{-1})	UG	10.	8.	−5.	−13.
	VG	10.	13.	1.	−3.
4. Surface heat flux F0(W m^{-2}) found from F0=F1·sin(πt/TC)+F2·t+F3	F1 (W m^{-2})	0	350.	280.	0
	F2 (W m^{-2})	0	0	0	0
	F3 (W m^{-2})	200.	0	0	6.
	TC (s)	1.	39600.	34200.	1.
5. Surface evaporation rate E0 (g m^{-2} s^{-1}) found from E0=E1·F0+E2·t+E3	E1 (g Ws^{-2})	0	0.0008	0.0001	0
	E2 (g m^{-2} s^{-2})	0	0	0	9
	E3 (g m^{-2} s^{-1})	0.03	0	0	0.1
6. Synoptic-scale subsidence (m s^{-1}) found from WS=$-B\cdot z$	B(s^{-1})	1×10^{-5}	$1.\times10^{-5}$	0.7×10^{-5}	2.6×10^{-5}
7. Surface pressure (mb)	P0	1000.	940.	1020.	1018.
8. Surface temperature (K) found from T=TSURFC·F0+$\hat{\theta}$	TSURFC (K m^2 W^{-1})	3.3×10^{-2})	3.3×10^{-2}	3.3×10^{-2}	1.0×10^{-2}
9. Cloud base vertical velocity (m s^{-1})	WCLD	1.0	1.0	1.0	1.0

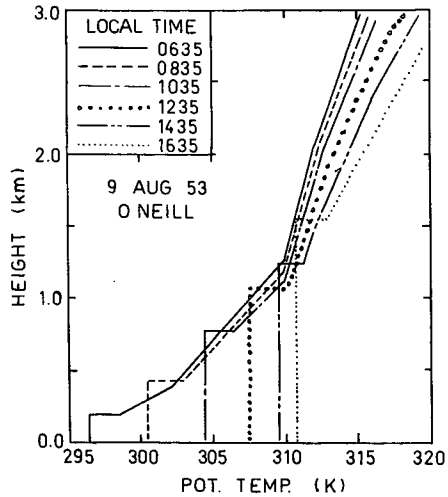

FIG. 2. Potential temperature profiles and inversion rise as calculated using the energetics inversion rise theory.

radiation, where

$$\frac{d\theta}{dt}=-w_s\frac{\partial\theta}{\partial z}+\frac{\theta}{C_pT}Q,\qquad \frac{d\rho_w}{dt}=-w_s\frac{\partial\rho_w}{\partial z}.$$

These basic equations are then used to calculate inversion rise and mixed layer depth, as is done in the next section for several cases.

3. Case studies

Inversion rise calculations based on the energetics entrainment theory were compared with observed atmospheric inversion rise for five cases (Stull, 1975). These cases were selected because advection, precipitation and frontal influences appeared to be small. Three of these observed cases are discussed in detail here. One case, 9 August 1953, is part of the Great Plains field experiment near O'Neill, Neb. (Lettau and Davidson, 1957); another, Day 33 (16 August 1967), is from the Australian Wangara field experiment near Hay (Clarke *et al.*, 1971); the last case is the suppressed tropical conditions found during the Puerto Rican experiment of 15 December 1972 (Pennell and LeMone, 1974).

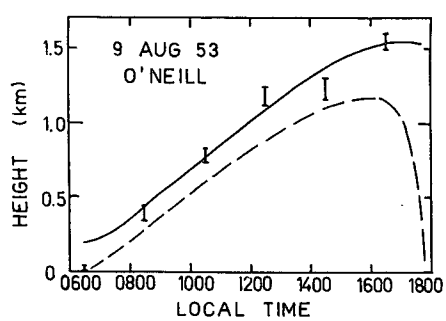

FIG. 3. Calculated inversion rise (solid line) compared with the observed rise (data bars) as a function of time. The dashed line shows the zero heat flux height.

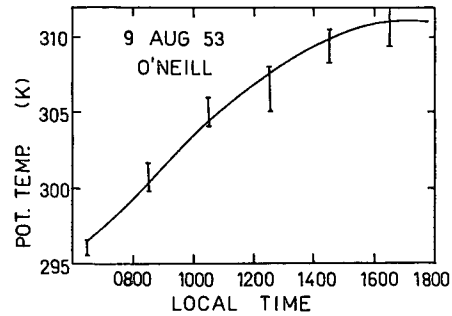

FIG. 4. Comparison of the calculated mixed layer mean potential temperature (solid line) with the observed values (data bars.)

In addition, a test was made of the sensitivity of the calculated inversion rise and mixed layer mean potential temperature to changes in the values of the coefficients of the energetics entrainment equation. Values for the boundary conditions, initial conditions, and other parameters for this sensitivity test and for the other cases are listed in Table 1. The initial profiles of potential temperature, humidity and geostrophic wind were chosen to be of nearly the same order of magnitude as is found in atmospheric situations.

It was found (Stull, 1975) that the calculated inversion height and potential temperature are most sensitive to changes in A_1. But even so, a 100% increase of A_1 from 0.1 to 0.2 results in only a 10% (20 m) increase in inversion height and a 3% (0.2°C) increase in potential temperature. In fact, the calculated inversion rise is most sensitive, in the atmospheric case, to the initial virtual potential temperature profile and the virtual heat flux at the earth's surface. That is, the thermodynamic environment usually dominates. So for a couple of cases to be described here, the calculated inversion rise based on the energetics theory is compared with that of the thermodynamics theory. In brief, the thermodynamics theory yields

$$\frac{\partial h}{\partial t}=\frac{(1+A_1)(\overline{w'\theta_v'})_s}{\gamma h}.$$

In another case, the calculations based on the full

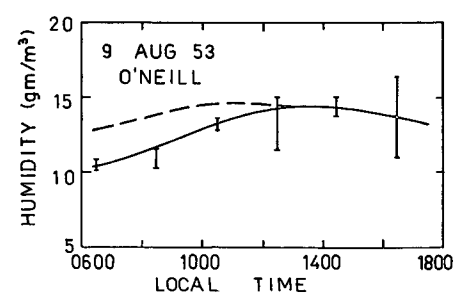

FIG. 5. Comparison of the calculated mixed layer mean humidity (solid line) with the observed values (data bars). The dashed line shows the saturation humidity at the top of the mixed layer.

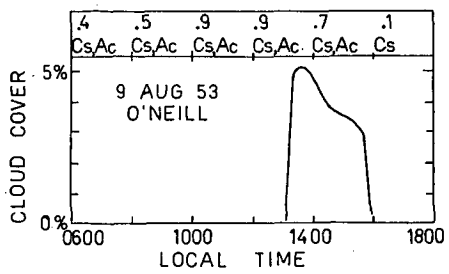

FIG. 6. Comparison of the calculated fraction of area covered by active convective clouds (lower portion of figure) with the reported cloud cover (upper portion).

energetics equation are compared with those using only the free convection part of the energetics equation.

a. Case 1: 9 August 1953, O'Neill

The observed temperature soundings are plotted in Fig. 1 for this late summer day. At 0635 local time there is a nocturnal inversion extending up to about 1200 m, above which is a nearly adiabatic region which was probably left from the mixed layer of the previous day. Later in the day, most of the soundings are nearly adiabatic up to the inversion base, except for the 1235 sounding, which was superadiabatic. The energetics theory requires that the mixed layer be adiabatic; hence, it is expected that the calculated inversion rise will be slightly off near 1235. Boundary and initial conditions are given in Table 1. Relatively strong winds (25 m s^{-1} at 500 m) and high humidities (11 g m^{-3} in the lowest 2 km) existed on this day, with clouds present.

The solid line in Fig. 2 shows the assumed initial temperature profile. Except for a thin layer near the surface, the assumed and observed profiles coincide.

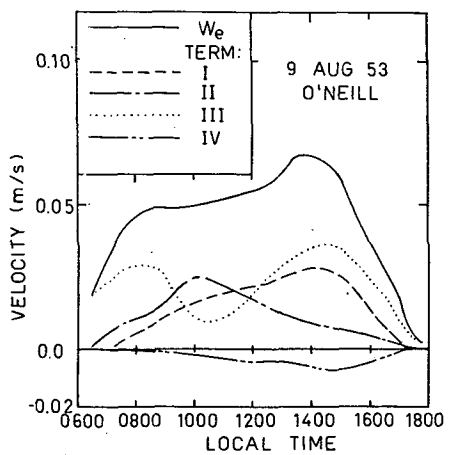

FIG. 7. Calculated contribution of each term in the energetics entrainment equation (1) to the total entrainment velocity (solid line). Term I is the buoyant contribution, term II is due to the wind shear at the earth's surface, term III is due to the wind shear at the inversion base, and term IV indicates the energy losses due to internal gravity waves.

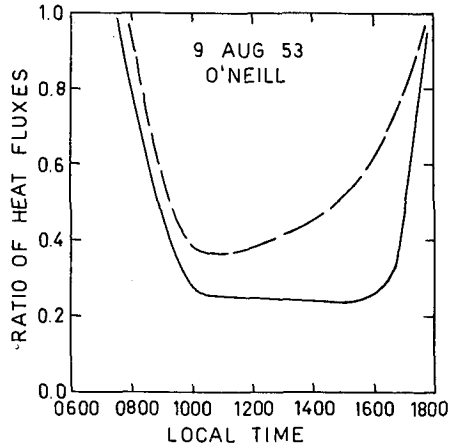

FIG. 8. Ratio of downward heat flux at the inversion base to upward heat flux at the earth's surface based on virtual potential temperature (solid line) and potential temperature (dashed line).

Near the surface this sounding is approximated with a shallow 200 m mixed layer with a 2 K jump in temperature at the top. This adiabatic region was assumed to enable the wind calculating routine in the computer program of the basic equations to converge. The temperature jump was chosen such that the heating required to fill in under this artificial mixed layer was equal to that required to fill in under the observed temperature profile. Hence, the net effect of this approximation quickly becomes negligible by the time the mixed layer has warmed by 2 K. Similar initial approximations are made for the other two cases.

Fig. 2 also shows the computed soundings during the course of the day, where both synoptic-scale and cloud-induced subsidence are seen to alter the upper levels. The computed inversion height and the level of zero heat flux as a function of time are plotted in Fig. 3, where it can be seen that, on the average, the computed inversion rise agrees with the observed rise. Similar agreement is found for the mean potential temperature of the mixed layer (Fig. 4).

Computed humidities, plotted in Fig. 5, agree in general with the observed values. The model calculates active convective cloud cover between 1300 and 1600 local time (Fig. 6). Agreement with reported clouds is poor. There is the possibility, however, that such clouds did occur and were either overlooked or classified as

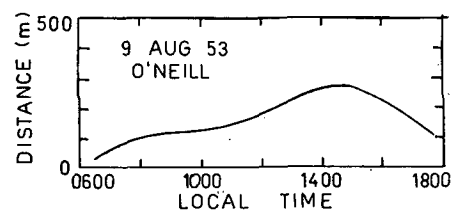

FIG. 9. Calculated overshoot distance d of the penetrative elements above the inversion base.

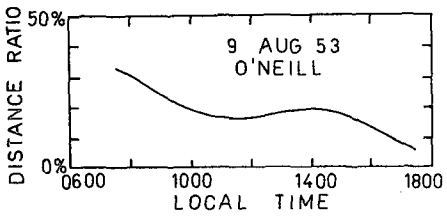

FIG. 10. Calculated ratio of the overshoot distance of the elements to the depth of the mixed layer.

altocumulus; the modeled cloud base is between 1.0 and 1.5 km. The calculated fraction of area covered by active clouds reaches only 5% in this case.

The importance of the various terms in the energetics entrainment equation [(1)] are shown in Fig. 7. For this case, all terms are of comparable magnitudes, although different terms dominate at different times. It must be concluded for this case that all terms of the energetics equation must be considered to adequately explain the inversion rise.

It is interesting to note from Fig. 8 that the ratio of downward virtual heat flux at the inversion base to upward flux at the surface is nearly constant at 0.25 from about 1000 to 1600 local time. This explains why theories in which only the buoyancy term of the energetics equation is used can successfully compute inversion rise given a large enough coefficient A_1; that is, such a theory would require that $A_1=0.25$ to yield successful results for this case. But $A_1=0.10$ was used here when considering the full energetics equation.

Also plotted in this figure is the same ratio based on potential temperature rather than virtual potential temperature. This exemplifies the large difference between the two ratios. Hence, they should not be used interchangeably.

Fig. 9 shows that the overshoot distance of the mixed layer convective/turbulent elements into the stable inversion increases as the mixed layer depth increases, as found in tank experiments by Deardorff *et al.* (1969). The overshoot reaches a maximum of about 250 m by 1500. Ratios of this distance to the inversion height, shown in Fig. 10, average about 20%. Noonkester's (1974) radar results show overshoot ratios ranging from 15 to 30%, with an average of about 23%.

Fig. 11 shows that the bulk Richardson number

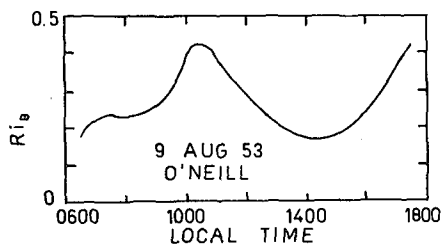

FIG. 11. Calculated bulk Richardson number at the inversion base.

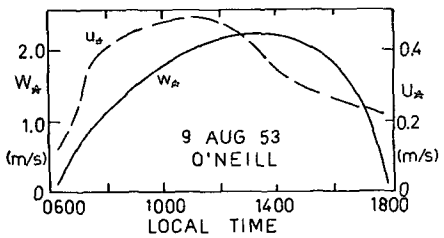

FIG. 12. Calculated values of the friction velocity u_* and the free convection scaling velocity w_*.

reached as low as 0.17 at 1430, which corresponds to the time of the maximum value of entrainment rate due to wind shear across the inversion and to the maximum of gravity wave energy losses. This suggests that the wind shear at the inversion base at that time could have not only supplied energy to the existing turbulent elements there, but could also have generated breaking Kelvin-Helmholtz instabilities. Furthermore, these K-H waves could have also contributed to the generation of internal gravity waves.

For background information, the computed values of u_* and w_* are plotted in Fig. 12. These values are within 20% of the observed values. The computed friction velocity u_* reaches a maximum near noon or late morning in all three O'Neill cases, whereas the free convection scaling velocity w_* peaks in the mid-afternoon. The potential temperature and virtual potential temperature jumps at the inversion base are plotted in Fig. 13. Again, note the large difference between the two; they should not be used interchangeably. Remember that the virtual potential temperature jump appears in the denominator of all of the terms in the energetics equation.

Two other O'Neill cases were tested (19 and 25 August 1953) by Stull (1975), although they are not discussed here. It was found that the calculated and observed inversion heights were in good agreement.

b. Case 2: Day 33, Wangara

Calculated profiles agree very well with the observed profiles for this case (Figs. 14–17). From Fig. 18 one sees that the buoyant contribution to entrainment velocity is the most important. This is to be expected because the winds are light. Remember that friction

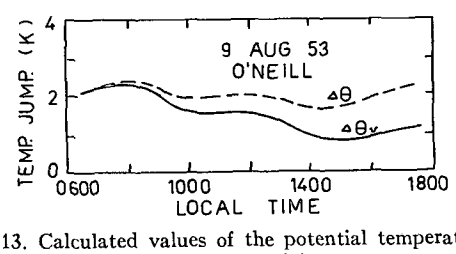

FIG. 13. Calculated values of the potential temperature step (dashed line) and the virtual potential temperature step (solid line) at the inversion base.

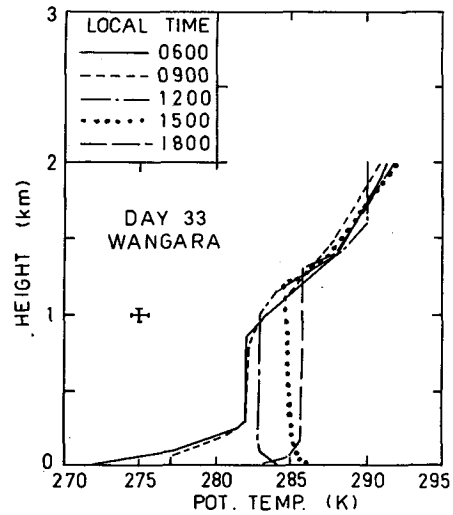

FIG. 14. As in Fig. 1 except for Wangara Day 33.

velocities and velocity jumps appear cubed in the energetics equation; this explains the large difference in relative magnitudes of the terms between this case and the previous case.

Due to the fact that the buoyant term dominates, one would expect that theories invoking only the buoyant term (free convection) would work quite well for this case. This method, slightly modified, was tested by Deardorff [1974a, his Eq. (27)] for Day 33. His assumed value for A_1 was too high (0.8) and, as expected, his calculated height by the end of the day was over 20% too great. Note that without his modification, his calculated inversion rise would have been even further off.

From Fig. 19 note that the daytime average of the virtual heat flux ratio was about 0.1. Hence, had Deardorff used this value, he would have probably

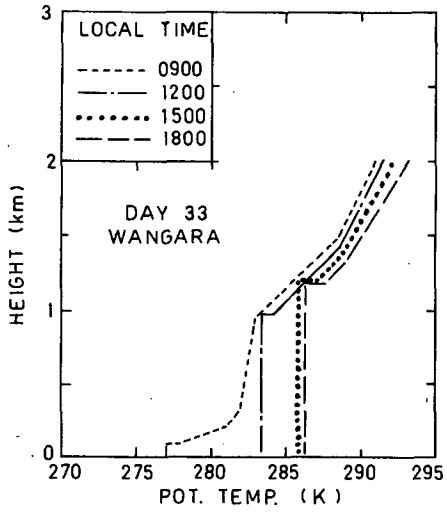

FIG. 15. As in Fig. 2 except for Wangara Day 33.

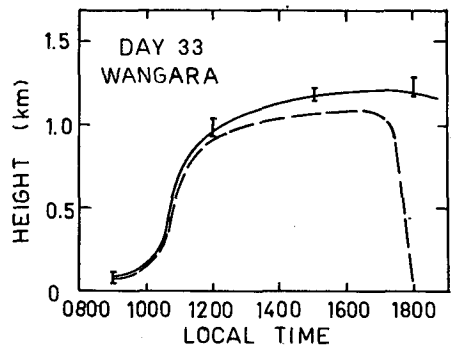

FIG. 16. As in Fig. 3 except for Wangara Day 33.

gotten much better agreement with the data. Fig. 20 shows the inversion heights calculated using the thermodynamics theory. Excellent results are obtained in this case because both the winds and the humidities are small. Thus, in similar atmospheric situations, it is much more economical to calculate inversion heights using the thermodynamics theory rather than the full energetics theory. The average penetrative element overshoot distance was 100 m on this day, while the ratio of overshoot to inversion height averaged 10%. Except in the early morning, the bulk Richardson number at the inversion was very large.

c. Case 3: 15 December 1972, Puerto Rico

Pennell and LeMone (1974) observed nearly steady-state cloud conditions in the tropics in one local suppressed region north of Puerto Rico. It is the purpose of this study to see if such a nearly steady-state cloud and inversion height situation could be simulated given the observed boundary layer data as initial and boundary conditions. It is assumed, following Betts (1973b) and Sarachik (1974), that the clouds can induce local subsidence around themselves, reinforcing the synoptic-scale subsidence. Additional data are listed in Table 2. Note that the subsidence velocity calculated from the divergence using synoptic charts could easily be an order of magnitude off.

Comparison of the assumed initial conditions and the observed profiles are shown in Fig. 21; the com-

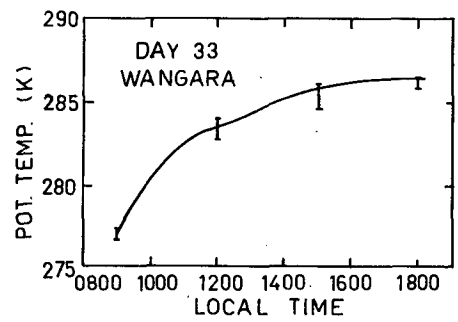

FIG. 17. As in Fig. 4 except for Wangara Day 33.

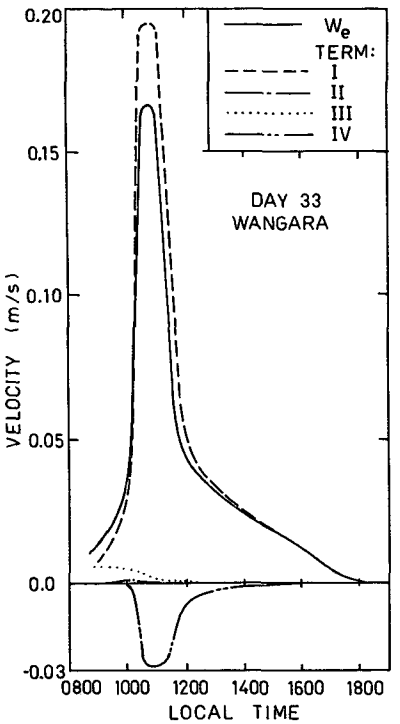

FIG. 18. As in Fig. 7 except for Wangara Day 33.

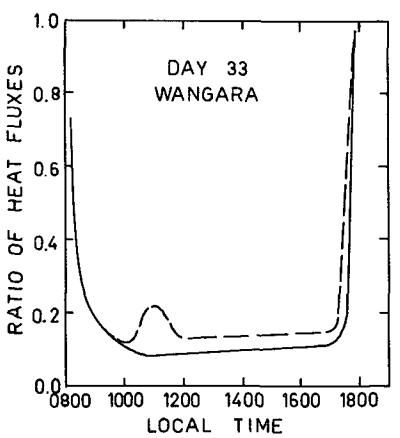

FIG. 19. As in Fig. 8 except for Wangara Day 33.

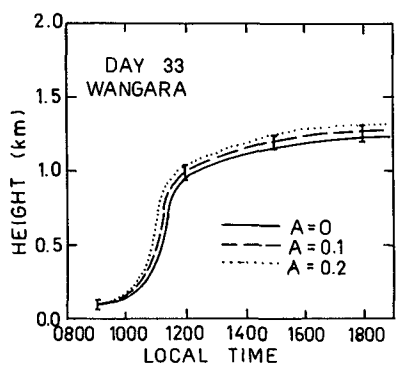

FIG. 20. Calculated inversion rise using the thermodynamics theory, where various values for the coefficient A_1 are tested.

TABLE 2. Steady-state magnitudes of the boundary conditions and other variables for the Puerto Rico case study.

Parameter	Value
u_*	0.25 m/s
w_*	0.73 m s^{-1}
Δu_h	4.1 m s^{-1}
w_s	−0.0156 m s^{-1}
Surface heat flux	6.0 W m^{-2}
Surface moisture flux	0.1 g m^{-2} s^{-1}
Surface virtual heat flux	24.0 W m^{-2}

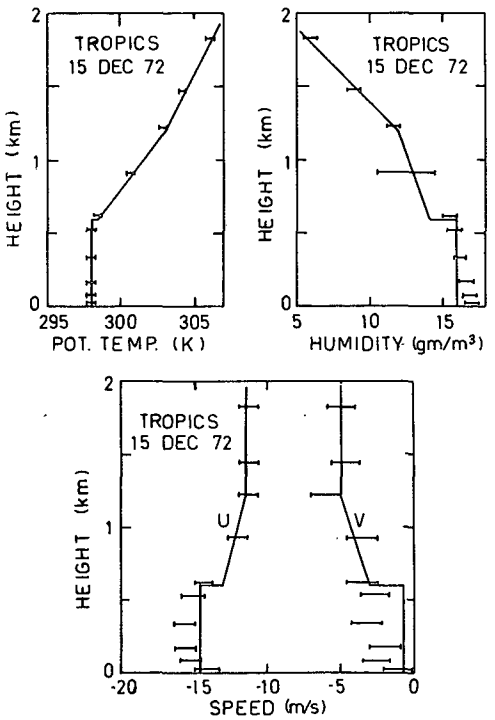

FIG. 21. Comparison of the observed potential temperature, humidity and wind speed profiles (data bars) with the assumed initial conditions for the calculation (solid lines).

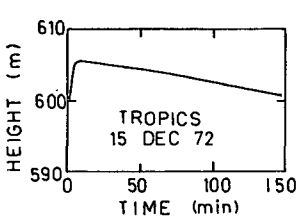

FIG. 22. Calculated inversion height.

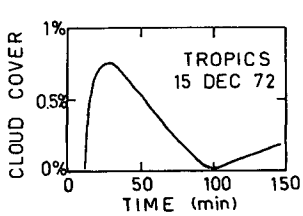

FIG. 23. Calculated cloud cover.

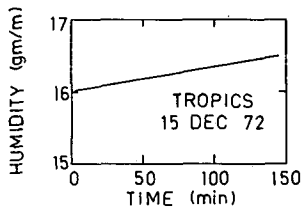

FIG. 24. Calculated mean mixed layer humidity.

puted inversion height is shown in Fig. 22. Initially cloud-free (Fig. 23), the inversion rises rapidly to about 605 m where clouds form. The inversion then descends very slowly back toward 600 m due to the additional cloud-induced subsidence. The inversion height changes by only 0.8% over a 2.5 h period; thus, a nearly steady-state condition was successfully simulated with cloud base in the observed height range (600–615 m). The computed mean mixed layer humidity and potential temperatures (Figs. 24 and 25) are also nearly in steady state.

To maintain this steady state, evaporation from the sea surface must be compensating the entrainment of dry air from above the cloud base, and heating due to entrainment of warm air and due to surface heat flux must be balanced by radiative cooling (neglecting advection).

Large wind shear effects on this day caused the ratio of virtual heat fluxes to be about 0.7 (Fig. 26). Fig. 27 shows that most of the energy causing entrainment is due to wind effects, with buoyant energy playing a minor roll. Gravity wave energy losses are also large. The resulting calculated entrainment velocities are only about 0.02 m s^{-1}. Hence, in the presence of a 0.015 m s^{-1} synoptic-scale subsidence velocity, a cloud-induced subsidence velocity of 0.0045 m s^{-1} is calculated to exist.

From Fig. 23, the fraction of area covered by active clouds is less than 0.5%, on the average. This is much less than the total observed convective cloud cover of 3 to 15%. This reflects the fact that cloud droplets remain visible long after the active cloud stage has ceased. Overshoot distances vary between 100 and 200 m, with an average ratio of overshoot distance to inversion height of roughly 20%. The calculated bulk Richardson number increases from 0.13 initially to 0.5 at the end of the period.

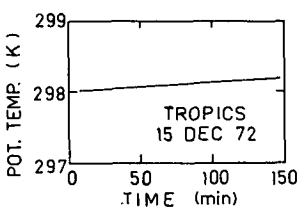

FIG. 25. Calculated mean mixed layer potential temperature.

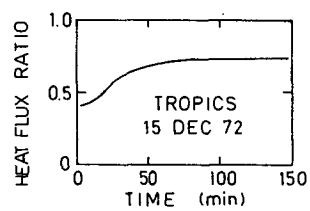

FIG. 26. Calculated ratio of downward heat flux at the inversion base to upward heat flux at the earth's surface.

4. Summary and conclusions

It has been shown in the companion papers (Stull, 1976a, b) that turbulent/convective elements overshooting into a temperature inversion from the mixed layer can cause entrainment of inversion air into that mixed layer. The mixed layer depth thus increases. Such an inversion rise is associated with an increase in potential energy of the inversion/mixed layer system. This energy comes from the turbulent kinetic energy of the mixed layer.

A diagnostic equation for the entrainment velocity based on this energetics theory was used. Starting with the turbulent kinetic energy (TKE) equation for the boundary layer, the time rate of potential energy change per unit area was related to mechanical and buoyant production of TKE, and to the internal gravity wave losses. Storage and viscous dissipation of TKE were assumed to be proportional to the production terms. An idealized atmospheric environment of an adiabatic mixed layer capped by a temperature step was assumed. This enabled the entrainment velocity equation to be written as a function of scaling velocities.

Many other published theories and experimental results concerning entrainment rates were shown to be

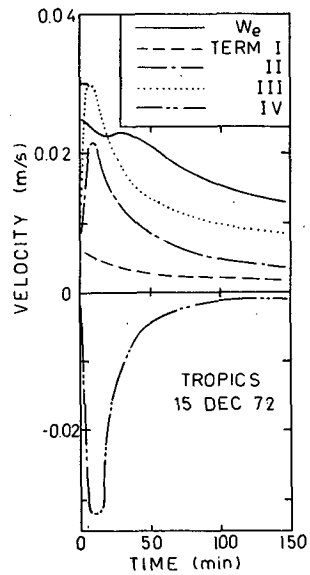

FIG. 27. As in Fig. 7 except for 15 December 1972, Puerto Rico.

special cases of this general energetics theory. This includes the inverse Richardson number relations, the dome-wisp theory, and theories assuming a magnitude for the ratio of downward to upward heat fluxes.

Budget equations are written in this paper which complete the atmospheric mixed layer depth model when closed with the entrainment equation. The influences of infrared radiation, gravity waves and clouds on inversion rise are included in the mixed layer model. Computations from the resulting atmospheric mixed layer model are tested with observations from several field experiments. These case studies indicate that, in general, the model does a very good job. Based on these successful results, the following conclusions are reached:

1) None of the terms of the entrainment rate equation should be neglected *a priori.*

2) The thermodynamics theory or just the buoyant part of the energetics theory are adequate when winds are weak (roughly, less than 5 m s^{-1} both below and just above the inversion base) and when solar heating is strong.

3) The full energetics equation describes tropical environments successfully.

4) Inversion rise is more sensitive in a given subsidence field to thermodynamic initial and boundary conditions than to values of the coefficients of the entrainment equation. Hence, it is very important to have accurate measurements of initial temperature and humidity profiles and of the heat and moisture fluxes during the day.

5) Ratios of downward buoyancy flux at the inversion to upward buoyancy flux near the earth's surface (and the corresponding heat fluxes) may vary from infinity at night to values <0.1 during the day, again depending on the situation.

6) Wind shear across a density interface can supply energy to pre-existing or externally created turbulence, even if the local Richardson number is not below its critical value.

7) Internal gravity wave energy losses are greatest when the inversion base wind shear contribution to entrainment rate is large.

8) Internal gravity wave energy losses can be important. They are often greatest when the Richardson number at the inversion is smallest, suggesting internal waves being associated with Kelvin-Helmholtz instabilities.

9) Internal gravity wave energy losses may limit the rise rate of inversions through regions that are nearly (but not exactly) adiabatic.

10) Local cloud-induced subsidence does appear as a mechanism for retarding the inversion rise rate.

11) At any one instant in time in a localized region, active convective clouds may comprise only a small percentage of the total observed convective cloud cover.

12) The transition layer just below tropical cloud base could be the region of overshoot of turbulent/convective elements above the inversion capping the subcloud layer.

During the testing of the energetics entrainment equation with field observations, values of the coefficients in the equations were set to give the best results. It must be emphasized that since these values were determined from a limited set of observations, they are by no means final. It is expected and desired that revisions be made to the values of these coefficients as more evidence is gathered from field and laboratory experiments. If possible, attempts should be made to obtain a theoretical prediction of their values.

The result found here that $A_1=0.10$ as opposed to recent literature values of $A_1=0.20$–0.30 is perhaps the most dramatic conclusion. This smaller value of A_1 reflects the importance of additional mechanisms besides free convection which can cause entrainment. Indeed, it is recommended that all mechanisms be considered when modeling or forecasting inversion rise, except possibly in cases of very light winds.

REFERENCES

Ball, F. K., 1960: Control of inversion height by surface heating. *Quart. J. Roy. Meteor. Soc.*, **86**, 48–494.

Betts, A. K., 1973a: Non-precipitating cumulus convection and its parameterization. *Quart. J. Roy. Meteor. Soc.*, **99**, 178–196.

——, 1973b: Notes on convection and the tropical boundary layer. Prepared for Boundary Layer-Convection Seminar (A GATE Workshop), University of Hamburg, 10–15 December. [Available from Dept. Atmos. Sci., Colorado State University].

Carson, D. J., 1973: The development of a dry inversion-capped convectively unstable boundary layer. *Quart. J. Roy. Meteor. Soc.*, **99**, 450–467.

Cattle, H., and K. H. Weston, 1973: The structure and development of the boundary layer over land in recent research in the U. K. on the atmospheric boundary layer and air/sea interaction. *Quart. J. Roy. Meteor. Soc.*, **99**, 767–768.

Clarke, R. H., A. J. Dyer, R. R. Brook, D. G. Reid and A. J. Troup, 1971: The Wangara Experiment: Boundary Layer Data. Tech. Paper No. 19, Div. Meteor. Phys., CSIRO, Melbourne, Australia, 350 pp.

Deardorff, J. W., 1968: Dependence of air-sea transfer coefficients on bulk stability. *J. Geophys. Res.*, **73**, 2549–2557.

——, 1973: An explanation of anomalously large Reynolds stresses within the convective planetary boundary layer. *J. Atmos. Sci.*, **30**, 1070–1076.

——, 1974a: Three-dimensional numerical study of the height and mean structure of a heated planetary boundary layer. *Boundary-Layer Meteor.*, **7**, 81–106.

——, 1974b: Three-dimensional numerical study of turbulence in an entraining mixed layer. *Boundary-Layer Meteor.*, **7**, 199–226.

——, and G. E. Willis, 1967: Investigation of turbulent thermal convection between horizontal plates. *J. Fluid Mech.*, **28**, 675–704.

——, G. E. Willis and D. K. Lilly, 1969: Laboratory investigation of non-steady penetrative convection. *J. Fluid Mech.*, **35**, 7–31.

Drake, R. L., P. D. Coyl and D. P. Anderson, 1975: Interactive line thermals in a convective layer: A numerical simulation. *J. Atmos. Sci.*, **32**, 302–319.

Fleagle, R. G., and J. A. Businger, 1963: *An Introduction to Atmospheric Physics.* Academic Press, 129–179.

Geisler, J. E., and E. B. Kraus, 1969: The well-mixed Ekman boundary layer. *Deep-Sea Res.*, **16**, Suppl., 73–84.

Izumi, Y., 1964: The evolution of temperature and velocity profiles during breakdown of a nocturnal investion and a low-level jet. *J. Appl. Meteor.*, **3**, 70–82.

Kraus, E. B., and J. S. Turner, 1967: A one-dimensional model of the seasonal thermocline. Part II. The general theory and its consequences. *Tellus*, **19**, 98–105.

Lenschow, D. H., 1970: Airplane measurements of planetary boundary layer structure. *J. Appl. Meteor.*, **9**, 874–884.

——, 1973: Two examples of planetary boundary layer modification over the Great Lakes. *J. Atmos. Sci.*, **30**, 568–581.

——, 1974: Model of the height variation of the turbulent kinetic energy budget in the unstable planetary boundary layer. *J. Atmos. Sci.*, **31**, 465–474.

Lettau, H. H., and B. Davidson, 1957: *Exploring the Atmosphere's First Mile*, Vol. 2. Pergamon Press, 578 pp.

Lilly, D. K., 1968: Models of cloud-topped mixed layers under a strong inversion. *Quart. J. Roy. Meteor. Soc.*, **94**, 292–309.

Mahrt, L., and D. H. Lenschow, 1976: Growth dynamics of the convectively mixed layer. *J. Atmos. Sci.*, **33**, 41–51.

Manton, M. J., 1975: Penetrative convection due to a field of thermals. *J. Atmos. Sci.*, **32**, 2272–2277.

McEwan, A. D., and G. W. Paltridge, 1976: Radiatively driven thermal convection bounded by an inversion—A laboratory simulation of stratus clouds. *J. Geophys. Res.*, **81**, 1095–1102.

Mendonca, B. G., and W. T. Iwaoka, 1969: The trade wind inversion at the slopes of Mauna Loa, Hawaii. *J. Appl. Meteor.*, **8**, 213–217.

Miropol'skiy, Y. A., 1970: Nonstationary model of the wind-convection mixing layer in the ocean. *Izv. Atmos. Oceanic Phys.*, **6**, 1284–1294.

Neiburger, M., D. S. Johnson and C. Chien, 1961: Studies of the structure of the atmosphere of the eastern Pacific ocean in summer. 1 The inversion of the eastern North Pacific Ocean. *Univ. Calif. Publ. Meteor.*, **1**, No. 1, 1–58.

Noonkester, V. R., 1974: Convective activity observed by FM-CW radar. TR 1919, Naval Electronics Laboratory Center, San Diego, 70 pp.

Orlanski, I., B. B. Ross and L. J. Polinsky, 1974: Diurnal variation of the planetary boundary layer in a mesoscale model. *J. Atmos. Sci.*, **31**, 965–989.

Pennell, W. T., and M. A. LeMone, 1974: An experimental study of turbulence structure in the fair-weather trade-wind boundary layer. *J. Atmos. Sci.*, **31**, 1308–1323.

Pollard, R. T., P. B. Phines and R. O. R. Y. Thompson, 1973: The deepending of the wind-mixed layer. *Geophys. Fluid Dyn.*, **3**, 381–404.

Rouse, H., and J. Dodu, 1955: Turbulent diffusion across a density discontinuity. *Houille Blanche*, **10**, 522–532.

Sarachik, E. S., 1974: The tropical mixed layer and cumulus parameterization. *J. Atmos. Sci.*, **31**, 2222–2225.

Staley, D. O., and G. M. Jurica, 1970: Flux emissivity tables for water vapor, carbon dioixde, and ozone. *J. Appl. Meteor.*, **9**, 365–373.

Stull, R. B., 1973: Inversion rise model based on penetrative convection. *J. Atmos. Sci.*, **30**, 1092–1099.

——, 1975: Temperature inversions capping atmospheric boundary layers. Ph.D. dissertation, University of Washington.

——, 1976a: The energetics of entrainment across a density interface. *J. Atmos. Sci.*, **33**, 1260–1267.

——, 1976b: Internal gravity waves generated by penetrative convection. *J. Atmos. Sci.*, **33**, 1279–1286.

Tennekes, H., 1973: A model for the dynamics of the inversion above a convective boundary layer. *J. Atmos. Sci.*, **30**, 558–567.

——, 1975: Reply (to Zilitinkevich). *J. Atmos. Sci.*, **32**, 992–996.

Turner, J. S., 1968: The influence of molecular diffusivity on turbulent entrainment across a density interface. *J. Fluid Mech.*, **33**, 639.

Willis, G. E., and J. W. Deardorff, 1974: A laboratory model of the unstable planetary boundary layer. *J. Atmos. Sci.*, **31**, 1297–1307.

Wyngaard, J. C., and O. R. Coté, 1974: The evolution of a convective boundary layer—A higher-order-closure model study. *Boundary Layer Meteor.*, **7**, 289–308.

Zilitinkevich, S. S., 1972: On the determination of the height of the Eckman boundary layer. *Boundary-Layer Meteor.*, **3**, 144–145.

——, 1975a: Resistance laws and prediction equations for the depth of the planetary boundary layer. *J. Atmos. Sci.*, **32**, 741–752.

——, 1975b: Comments on "A model for the dynamics of the inversion above a convective boundary layer." *J. Atmos. Sci.*, **32**, 991–992.

——, and J. W. Deardorff, 1974: Similarity theory for the planetary boundary layer of time-dependent height. *J. Atmos. Sci.*, **31**, 1449–1452.